NAVIER-STOKES CALCULATIONS OF THE FLOW ABOUT WING-FLAP COMBINATIONS

A. Kogan , S. Marom(Migemi)
Tashan Engineering Center
Israel Aicraft Industries

Abstract

The Baldwin-Lomax turbulence model incorporated into The Navier-Stokes code FIDAP is used to calculate C_L vs. α curves for wing-flap combinations up to C_{Lmax}. The flow solution shows wiggles in Cp and computed C_L is low. Better agreement with experiment is obtained when the wiggles are suppressed by applying the slip condition in laminar regions. In addition, tuning the penalty and upwinding parameters results in still better agreement with experiments. The agreement with experiments over Foster,GA(W),NLR multi-elements depends on the test conditions such as model , suction and blowing. The agreement of computed and experimental Cp for laminar PR8 multi-element at 1.5 Re is reasonable at the same C_L . The discrepancy between computed and experimental α increases with C_L . For 1 million Re we use a procedure to compute bubble development and Cp. Whenever possible, results are compared to experiments and the agreement is reasonable.

Introduction

In this paper we treat the viscous flow about two-dimensional multi-elements composed of a wing and a back flap. The main interest is in exterior flows with high Reynolds numbers which are mainly turbulent. We restrict our attention to steady incompressible flows. The viscous laminar flow is governed by the steady Navier-Stokes and continuity equations

$$u_k \frac{\partial u_i}{\partial x_k} + \frac{1}{\rho}\frac{\partial p}{\partial x_i} = \frac{\partial}{\partial x_k}\left[\nu\left(\frac{\partial u_i}{\partial x_k} + \frac{\partial u_k}{\partial x_i}\right)\right] \quad (1)$$

$$\frac{\partial u_k}{\partial x_k} = 0 \quad (2)$$

For high Reynolds number flows the laminar boundary layer is absolutely unstable and undergoes transition to turbulence. Equations (1),(2) are not directly soluble for turbulent flows and as usual we use the time-averaged form of these equations:

$$\bar{u}_k \frac{\partial \bar{u}_i}{\partial x_k} + \frac{1}{\rho}\frac{\partial \bar{p}}{\partial x_i} = \frac{\partial}{\partial x_k}\left[\nu\left(\frac{\partial \bar{u}_i}{\partial x_k} + \frac{\partial \bar{u}_k}{\partial x_i}\right) - \overline{u_i' u_k'}\right] \quad (3)$$

$$\frac{\partial \bar{u}_k}{\partial x_k} = 0 \quad (4)$$

The Reynolds turbulent stress-tensor

$$R_{ik} = -\overline{u_i' u_k'} \quad (5)$$

describes the influence of the fluctuating motion on the average motion. To close system (3) through (5), we must express R_{ik} in terms of mean flow quantities For convenience we drop the bar denoting mean values and all variables appearing below are mean flow quantities.

In a previous paper[1] we have described the inclusion of the Baldwin-Lomax algebraic turbulence model[2] into the incompressible Navier-Stoke finite-elements code FIDAP[3].

We presented[1] applications of the model to the prediction of C_{Lmax} for NACA0012, NACA4415 airfoils and to the computation of the turbulent flow about an airfoil with laminar separation bubble. Whenever possible comparison of computed Cp distribution and C_L to experiments were made and the agreement was reasonable. In this report we extend the application of the Baldwin-Lomax model incorporated into FIDAP to turbulent flows about 2-D wing-flap combinations. The turbulent flow about a wing-flap combination is much more complex than the flow about a single airfoil for a number of reasons. First, the more complex geometry, including the channel between the wing and the flap, makes more complex flow patterns possible. Secondly, the very high C_L values are associated mostly with high pressure peaks at the leading edge of the wing. This subjects the boundary layer to large adverse pressure gradients and the downstream development of the boundary layer is more difficult to predict. In addition, there might be interactions among the boundary layers/wakes of the wing with those developing on the flap. For most practical wing-flap combinations the highest C_{Lmax} are obtained for gap values about 2% of the basic

wing chord. Therefore, we consider mainly geometries with wing-flap gap values around these values.

When trying to calculate the flow over Foster multi-element[4] we get wiggles[5] in Cp and the computed C_L is much smaller than the experimental C_L. We suppress the wiggles in Cp by allowing the flow to slip in the laminar boundary layer region. As a result the wiggles in Cp disappear and the computed C_L is higher. In order to improve further the comparison with experiment it is necessary to tune up the penalty parameter β defined in equ.(7) below and the upwinding parameter. The comparison of computed C_L with C_L measured in a later experiment[6] on the same configuration gives a much better agreement. The differences between the experiments [4] and [6] is in the wind tunnels models and test conditions used to achieve two dimensional flow conditions.

Next we consider the GA (W) - 1 wing-flap combination for two flap deflections of 10 and 40 degrees[7]. Again, we suppress the wiggles in Cp by allowing the flow to slip in the laminar portion of the boundary layer on the wing and flap surfaces. In addition, we tune up the penalty parameter in order to compute the turbulent flow for various angles of attack. The predicted C_L versus α curve for 40 degrees flap deflection is in good agreement with experiment.

For the wing-flap geometry with 10 degrees flap deflection flow computations show attached flow over the flap and wing up to C_{Lmax} with flow separation in the wake leading to C_{Lmax} and to stall.

Flow visualization results[7] confirm the turbulent flow separation characteristics for both flap deflections as predicted by the flow computations.

Next, computed results are compared to the experiment by Van den Berg[9] on NLR wing-flap combination, designed so that flow separation occurred nowhere on the surface even close to C_{Lmax}. The computed and the experimental C_L vs. α curves are in good agreement. The computations predict no separation everywhere on the surfaces also close to C_{Lmax} and predict wake separation leading to stall and to C_{Lmax}. The comparison of the computed C_L vs. α curve to the curve computed by Cebeci[10] using an interaction method shows the advantages of using a Navier-Stokes code to predict C_{Lmax} and flow separations.

In our previous work[1] we described a procedure to predict laminar bubble development over laminar airfoils. The main feature of this laminar bubble simulation is that bubble location and Cp is predicted directly using the full Navier-Stokes code as opposed to other methods that predict bubble development by considering the interaction of the viscid flow with the external inviscid flow. First, we apply this procedure to the turbulent flows about a wing-flap combination with laminar airfoil PR8 as the main wing. The PR8 airfoil was designed and tested at IAI. In this case the laminar boundary layer is well developed, there are no wiggles in Cp and the no-slip condition is applied on all solid surfaces.

The comparison of computed Cp with experimental Cp at Re of 1.5 millions at the same C_L shows good agreement. The discrepancy between the corresponding angles of attack increase with C_L.Such a high discrepancy in α was not observed in the case of Foster and GA (W)-1 wing-flap combinations.This discrepancy would be further disscussed below. We compare computed results to available experimental results at Re of 1 million. We compute the flow at Re number of 1 million about the same geometry for α of 8 degrees. The comparison of computed velocity inside the turbulent boundary layer with measured velocity in the wing upper trailing edge region shows good agreement. A by-product of the laminar bubble simulation at 1 million Re number is an improved prediction method for bubble location and Cp distribution.

The Numerical Method

As the basic Navier-Stokes code we have applied FIDAP[3] with the algebraic model incorporated into it. FIDAP is a finite element code for the incompressible Navier-Stokes equations. For turbulent steady flows the equations of conservation of momentum are written in the stress divergence form

$$\rho\, u_k \frac{\partial u_i}{\partial x_k} = \frac{\partial \tau_{ik}}{\partial x_k}$$

$$\tau_{ik} = -p\,\delta_{ik} + \mu\left(\frac{\partial u_i}{\partial x_k} + \frac{\partial u_k}{\partial x_i}\right) \qquad (6)$$

For simplicity, instead of the continuity equation (4) we use the pressure penalization

$$p = \frac{1}{\beta}\frac{\partial u_k}{\partial x_k} \qquad (7)$$

with penalty parameter β=1.E-8 1.E-7. Equations (6),(7) are solved by the Galerkin method in the finite element approximation. The resulting system is solved by the method of successive approximations.

Upwinding

High Reynolds number flows are flows with small molecular viscosity. The artificial viscosity (upwinding) added for numerical stability may wholly misrepresent the structures and scales of turbulent boundary layers to give a wrong flow picture. In FIDAP the artificial viscosity has the form of streamline upwinding. This means that the longitudinal artificial

stress

$$\mu_{art} \frac{\partial u}{\partial x} \tag{8}$$

where μ_{art} is proportional to the mesh size δx, is added to the molecular stress

$$\mu \frac{\partial u}{\partial x} \tag{9}$$

On the other hand, there is no contribution of artificial viscosity to the real shear normal stress

$$\mu \frac{\partial u}{\partial y} \tag{10}$$

acting across the boundary layer. Consequently the artificial viscosity does not effect the turbulent viscosity coefficient in the Baldwin -Lomax model .

The longitudinal derivative of the artificial stress (∂/∂_x) $(\mu_{art}\, \partial u/\partial x)$, adds an artificial force to the pressure gradient and to some extent this may have an influence on the separation point of the aerofoil. To reduce this effect it is necessary to refine the mesh in the longitudinal direction. As will be described upwinding has some influence on C_L and Cp distribution for wing-flap combinations.

Grid Generation for Multi-Elements

For a single airfoil the typical grid is a C grid and about 7000 grid points are used to calculate the turbulent boundary layer. It is important for a wing-flap configuration to use a small number of points as possible. For example, if the number of grid points is increased from 10000 to 11000 the computer time is increased by 30% because of the increase of up to 1000 in band width of the finite element matrix.

For this reason we use for a multi-element case a H-C grid topology as in Fig. 1 . A local C grid which includes the boundary layer developing about the component at high Reynolds number is attached to every component. These local C grids are imbedded in a global H grid. These type of H-C topology allows us to separate the grid points above/below the configuration from those below/above the configuration by connecting them to upper/lower horizontal lines of the H grid. In this case we use a much lower number of horizontal grid lines in the upper part than in the lower part, where it is necessary to use a relatively high number of grid points because of the slot region. The number of grid points used (11000) is between 1/2 and 1/3 of the number of grid points used by Navier-Stokes codes using finite differences to compute flows about multi-elements.

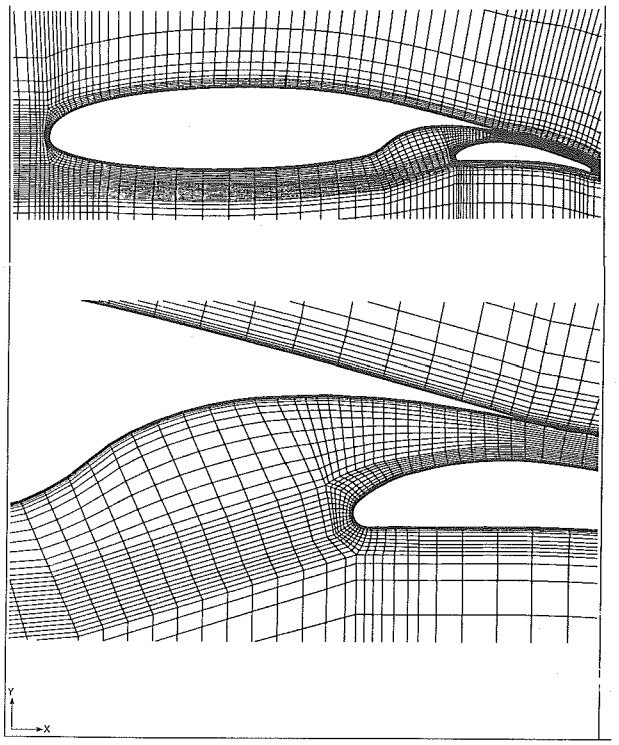

Fig. 1 H-C grid generation for turbulent flow. GA(W)-1 multi - element.

To resolve the thin turbulent boundary layer we must have high grid resolution normal to the surface. Usually the height δy of the first cell above the airfoil is 0.00002C, where C is the basic wing chord. As noted, the grid lines are locally orthogonal to the surface within the boundary layer. On the average 20 grid points are used inside the boundary layer out of a total of 36 points in the y-direction.

Boundary and Initial Conditions

A sketch of the computational domain is given in Fig. 2. The wing-flap combination is placed inside the computational domain. At infinity the computational domain is bounded by lines HI and GJ about 6 aerofoil chords away from the aerofoil. The top and bottom boundaries are 6 chords away from the aerofoil. For incompressible flow the pressure is defined up to an additive constant. Since the velocity is a constant vector at infinity, it follows from (7) that the constant is defined in such a way that

$$p\ (\infty) = 0 \tag{11}$$

On the wing ABC and flap DEF we have the no-slip condition

$$u_i|_{ABC} = 0\ ,\ u_i|_{DEF} = 0 \tag{12}$$

On the part GHI that is an inflow boundary of the far field boundary we prescribe the free velocity condition

$$\begin{aligned} u_1\ (\infty) &= u_\infty \cos(\alpha) \\ u_2\ (\infty) &= u_\infty \sin(\alpha) \end{aligned} \tag{13}$$

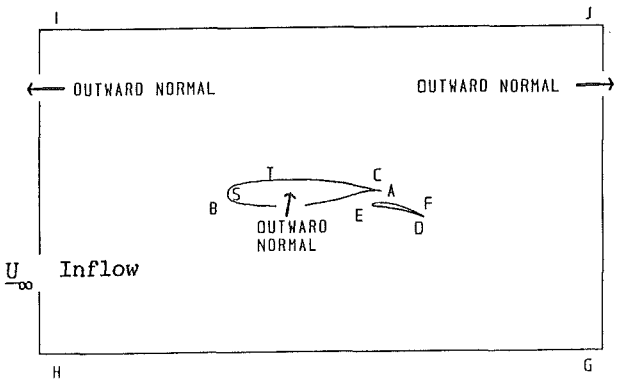

Fig. 2 Computational domain for Navier-Stokes calculations for wing-flap configuration.

where U_∞ is the velocity at infinity and α is the angle of attack. On the parts GJ,IJ normal zero-stress conditions are applied:

$$\tau_{ik}\, n_k = \left[-p\, n_i + \mu \left(\frac{\partial u_i}{\partial x_k} + \frac{\partial u_k}{\partial x_i} \right) n_k \right]_\infty = 0 \qquad (14)$$

In case we allow the flow to slip over the surface in the laminar region between the stagnation points S and the transition points T, (12) applies only to the velocity component normal to the surface.

The Turbulence Model

To express the Reynolds stresses R_{ik} by means of mean velocities we use the Boussinesq eddy viscosity concept:

$$-\overline{u_i' u_k'} = \nu_t(x_1,x_2) \left(\frac{\partial u_i}{\partial x_k} + \frac{\partial u_k}{\partial x_i} \right) \quad i = 1,2 \qquad (15)$$

The turbulent viscosity coefficient $\nu_t(x_1,x_2)$ is defined semi-empirically by the Baldwin-Lomax model. As noted, the Baldwin-Lomax model is used in all the computations given below. In the flow domain we generate groups of quadrilateral finite-elements within which the model is separately applied. There is no interaction between the viscosities $\nu_t(x_1,x_2)$ defined in the different groups. The definition of the groups follows the viscous flow development over the different components. For example, both for the wing and the flap two groups of elements are defined. One group of elements starts at the leading edge and extends along the upper surface and the upper wake of that component. The group extends far enough into the flow to include the boundary layer and wake. Since the Baldwin-Lomax model defines the turbulent viscosities in terms of a coordinate system that is locally orthogonal to the surface, the grid lines in each group are locally orthogonal to the surface.
In case the wing or the flap have blunt trailing edge, we generate a group of elements having the trailing edge as a base. However, since the bluntness considered is small the model is not applied there.

Outside the groups where the model is applied the viscosity is equal to the molecular viscosity only . This way of applying the model resulted in a practical method to calculate separated flows over airfoils up to C_{Lmax}. In the present work we apply the model to turbulent flows over wing-flap combinations with at most weak interaction among the boundary layers /wakes of the different components. Fortunately, for most if not all practical wing-flap combinations the viscous interaction at the optimal geometry and flow conditions is weak. In any case, by post-processing the computed velocity field the assumption of weak interaction may be verified and the application of the model justified.

Results

Results of the calculations of turbulent flows over a number of wing-flap combinations are presented below. For each configuration we predict C_{Lmax} directly by computing the flow for a sequence of angles of attacks up to and slightly above C_{Lmax}. This direct prediction capability is one of the main advantages of a full Navier-Stokes solver code over codes that solve the flows over wing-flap combinations using inviscid/viscid flow interaction methods. Whenever possible, computed results are compared to experiment.

Foster Multi-Element

The basic wing section of a wing-flap combination tested by Foster[4] is a RAE 2815.The flap chord is 40% of the wing chord. The shroud TE is at 87% wing chord. The configuration was tested for 10°,30° flap deflections at Re number of 3.8 million and for wing-flap gap values between 1.5%-2.5%. The model included the wing-flap as a uniform section and was mounted between the wind tunnel walls. Suction was used to establish two-dimensional flow conditions and to prevent separation. We compute at Re of 3.8 million the flows for flap deflections of 10 degrees with 3.1% overlap and 2.5% gap values (Fig. 3). For all the computations transition on the flap surfaces is fixed at the experimental transition points. On the wing surfaces the transition is fixed at the laminar separation points obtained by computing the laminar flow at the same Re and α.

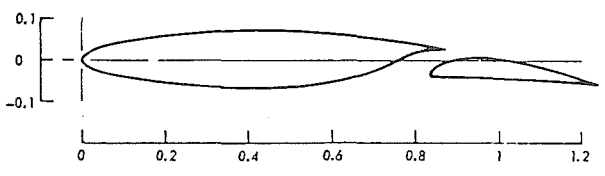

Fig. 3 Foster multi-element, δ_f = 10 degrees.

RAE 2815 Airfoil, 40 percent flap.

The computed solutions show wiggles in Cp. The wiggles occur on all wing and flap surfaces and they are largest at the wing leading edge region, where the peaks in Cp develop with increasing α. The wiggles in Cp on the wing upper surface are given in Fig. 4. Because of the wiggles in Cp the computed C_L for α of 2° is 0.95 and for 9° is 1.68, and is much lower than the experimental values of 1.3 and 2.0 respectively. Although the occurence of wiggles in Cp when solving the incompressible Navier-Stokes equations using finite-elements with the penalty approach (equation (7)) is well known , we believe their significant effect on practical turbulent high lift flows over wing-flap combinations is a new observation. In case of a turbulent flat plate at zero incidence the wiggles in C_p are almost symmetrical about zero giving C_L very close to zero as should be. In this case and in the case of flows over airfoils there is no moticeable effect on C_L. The methods suggested[5] to filter out the correct Cp are not useful in our case because of the large amplitude of the wiggles. We tried grid refinement along and normal to the surface, but this had no effect on the wiggles in Cp.

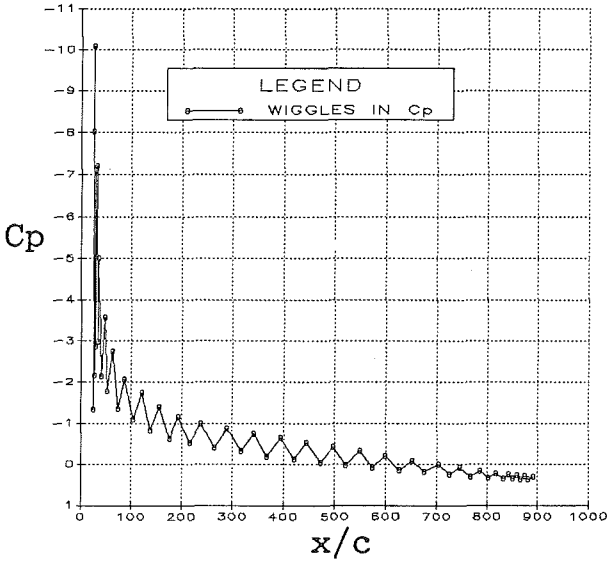

Fig. 4 Wiggles in Cp at wing's leading edge.

Re = 3.8 million , α = 9 degrees.

To analyse the reason for the Cp oscillations we plot the velocity vector paralell to the surface for α of 9 degrees (Fig. 5). We see that on the main wing surface at the leading edge there is not a velocity profile typical to laminar boundary layer. The velocity at the surface is zero by the no-slip condition and at the next grid point off the surface the velocity has almost the value of the external flow velocity.

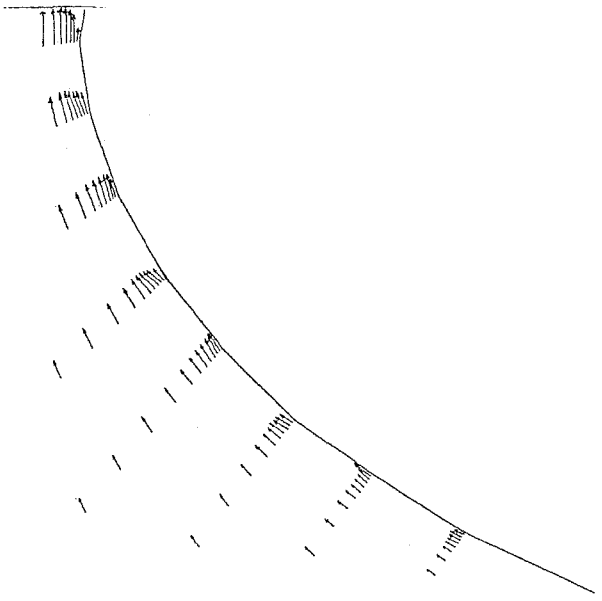

Fig. 5 Velocity plot in the laminar region at the leading edge of the wing.
Re = 3.8 million, α = 9 degrees.

The reason is that the laminar boundary layer developing from the stagnation point is so thin that the grid resolution normal to the body is incapable of resolving the laminar flow close to the surface. In fact, the first grid point off the surface at the leading edge is outside the laminar layer there. The use of the no-slip condition to get the laminar flow without having grid points inside the very thin laminar layer causes great oscillations in Cp and a significant loss of lift. If the grid resolution used in practice is unable to resolve the laminar layer we have to give up the no-slip condition. Therefore from the stagnation point up to the fixed transition point on the wing/flap upper surface we use the slip condition. Elsewhere we use the no-slip condition as usual. When computing the turbulent flow over the multi-element with the modified boundary condition the Cp oscillations at the leading edge disappear and elsewhere the oscillations become smaller.

For α of 9° transition is fixed at 2% chord on the wing upper surface and at 18% chord on the wing lower surface. On the flap upper surface transition is fixed at 8% flap chord and on the lower surface at 40% chord flap chord. Comparison of computed Cp to experiment is shown in Fig. 6. It is seen that the agreement is reasonable.

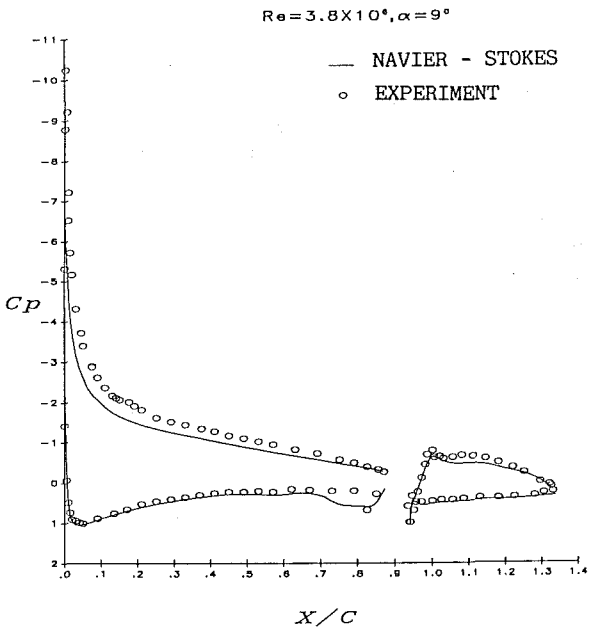

Fig. 6 Comparison of computed Cp to experiment. δ_f =10 degrees, α = 9 degrees.

A series of calculations for the 10 degrees flap deflection gives C_L versus α curve. The streamlines of the flow and the Cp distribution over the Foster multi-element configuration for α of 11,12.5,13 degrees is given in Fig. 7. It is seen that for angles of attack of 11,12.5 degrees there is trailing edge separation on the main airfoil, but the flow over the flap is attached. At 13 degrees angle of attack there is massive separation typical to post C_{Lmax} stall. The experimental C_L versus α curve and the C_L versus α curve for the calculation with and without the no-slip condition are also given in Fig. 8. It is seen that the C_{Lmax} predicted with the slip condition at the leading edge is 2.0 whereas the experimental value is 2.16. The C_{Lmax} predicted with the no-slip condition is only 1.71.
At a later stage we became aware of an experiment at NASA AMES on the same configuration. The model tested was a high aspect ratio rectangular wing with the wing-flap as a uniform section, so that two-dimensional flow conditions were established over the wing center section. This avoids the interference effects with the tunnel walls and avoids the need for blowing or suction as was in Foster's experiment. In this experiment the measured C_L for α of 9° is 1.9. Therefore, we repeated the computation for α of 9°. In this computation we tune up the value of penalty parameter β (equ. (7)) and the computed C_L is 1.87.

Since the accuracy of Cp (and hence C_L) calculation depend on β being small the tuning is simple and we take smallest β for which the iterations converge.

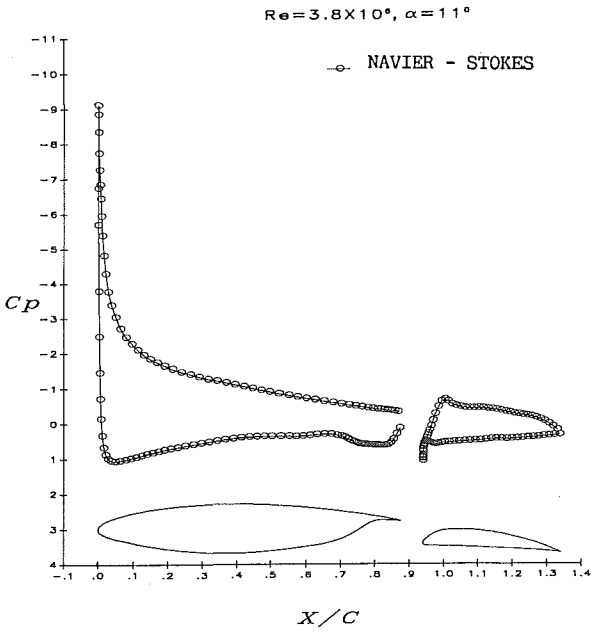

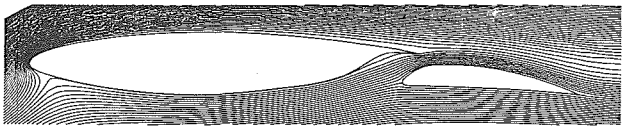

Fig. 7 (a) Foster configuration streamlines, Cp. Re = 3.8 million, α = 11°.

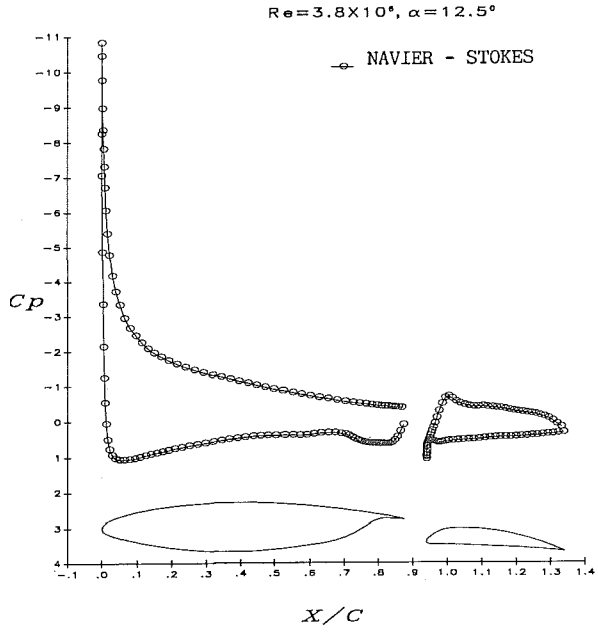

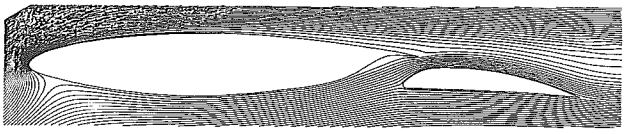

Fig. 7 (b) Foster configuration streamlines, Cp. Re = 3.8 million, α = 12.5°.

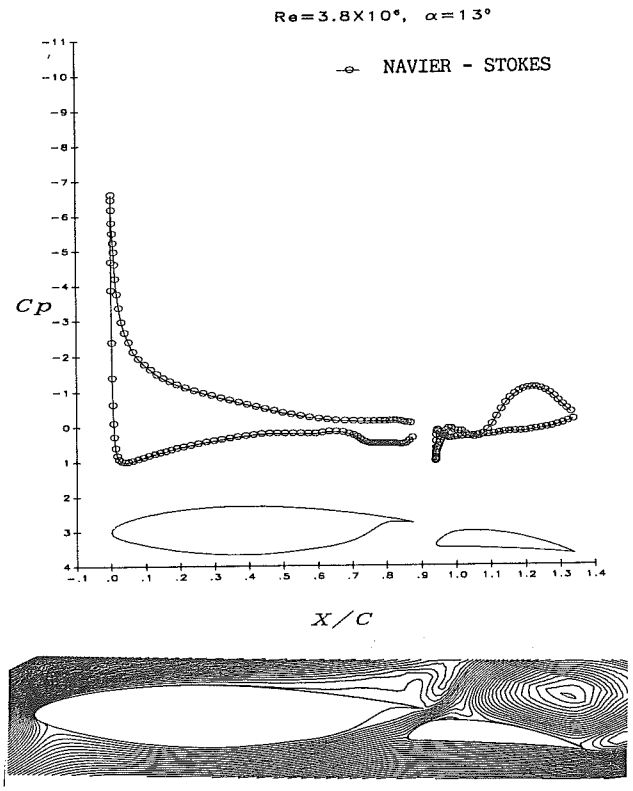

Fig. 7 (c) Foster configuration streamlines, Cp. Re = 3.8 million, α = 13°.

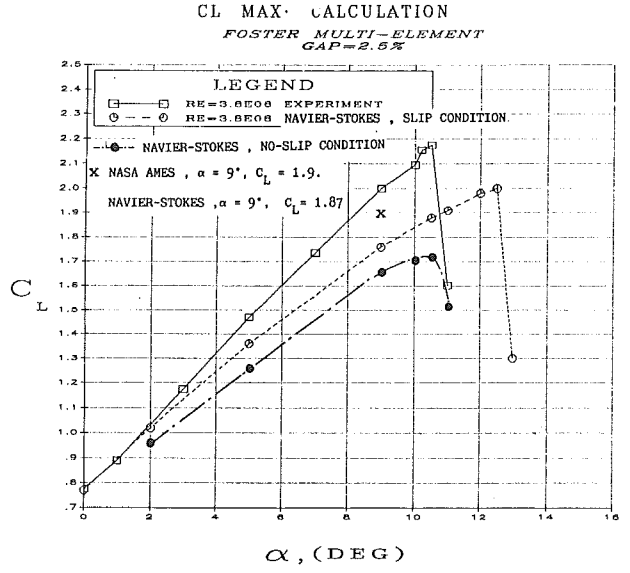

Fig. 8 Comparison of C_L vs. α curve computed with/without slip codition to experiment.

GA (W) - 1 Multi-Element

the GA (W) - 1 multi-element has a supercritical wing section and was tested in a Low Speed Tunnel with two-dimensional Insert. Therefore, neither suction nor blowing were used to establish two-dimensional flow conditions. For comparison with experiment we compute the flow for the wing-flap combination with 29 % basic wing chord flap and flap deflection of 40 and 10 degrees. The Re number is 2.2 millions for both the experiment and the calculation.

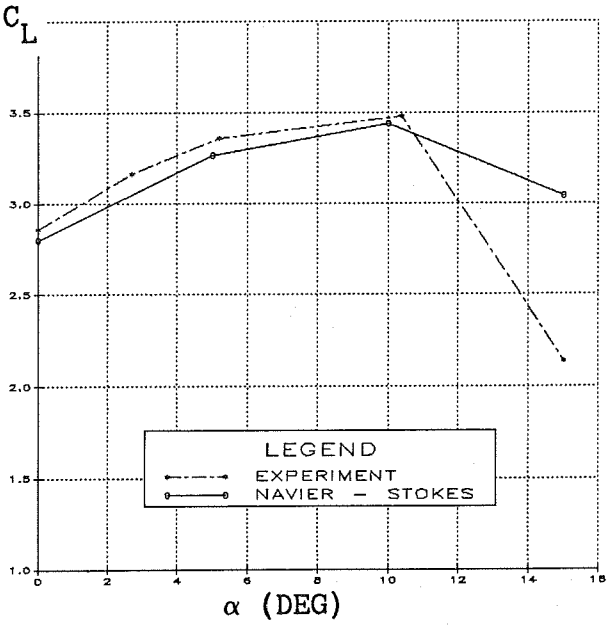

Fig. 9 Comparison of computed C_L vs. α curve to experiment for GA(W)-1 multi-element. Re = 2.2 million, δ_f = 40°.

For the 40 degrees flap deflection the gap is 2.7% and the overlap is 1.7% basic wing chord. A sequence of computations for δ_f =40 degrees gave the C_{Lmax} vs. α curve which is compared to experimental curve in Fig. 9. In these calculations we apply the slip condition in the laminar regions on the wing and flap upper surfaces and tune up the penalty and the upwinding parameters as disscussed above. It is seen that the agreement is quite good with computed C_{Lmax} of 3.42 at 10 degrees angle of attack very close to experimental C_{Lmax} of 3.46 at 10.4 degrees angle of attack. Again, since no blowing was used the computed and the experimental C_L vs. α curves are in quite good agreement.

The streamlines and Cp for 0,10,15. degrees angles of attack are shown in Fig.10,Fig.11 and Fig.12 respectively. For zero angle of attack it is seen that the flow over the flap is separated near the trailng edge with the Cp having a flat portion there ,whereas the flow over the wing is attached. This is evident also from flow visualization using tufts[7]. As the angle of attack is increased the flow over the flap is attached and flow separation begins in the wake .

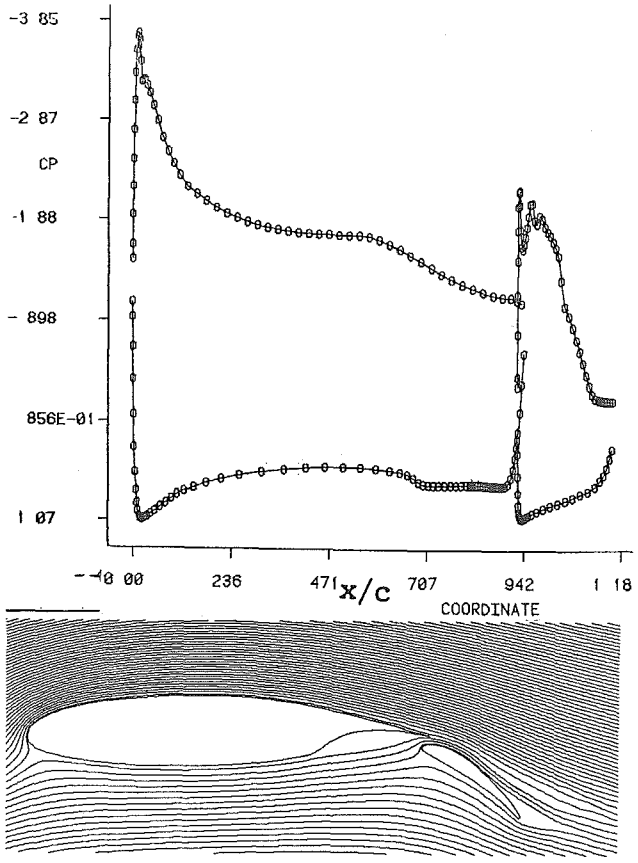

Fig.10 Streamlines and Cp, α = 0°, δ_f = 40°. GA(W)-1 multi-element.

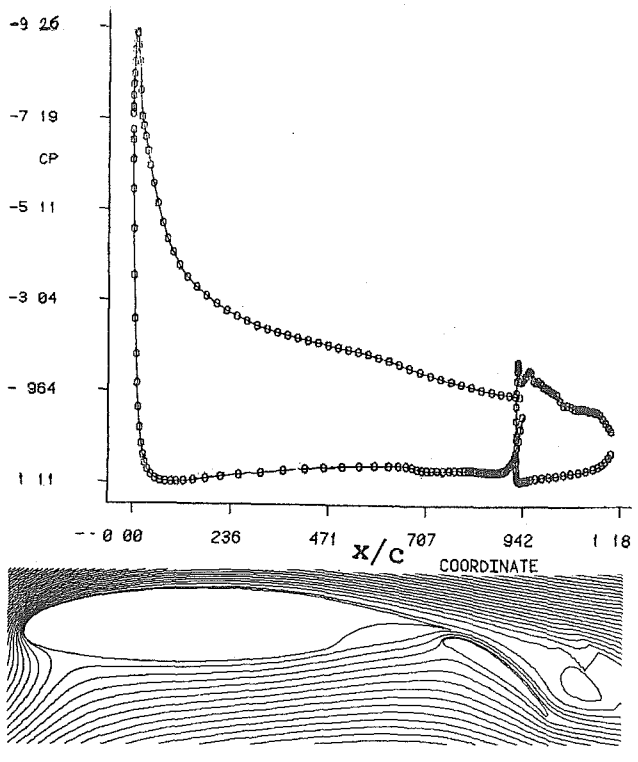

Fig.11 Streamlines and Cp, α = 10°, δ_f = 40°. GA(W)-1 multi-element.

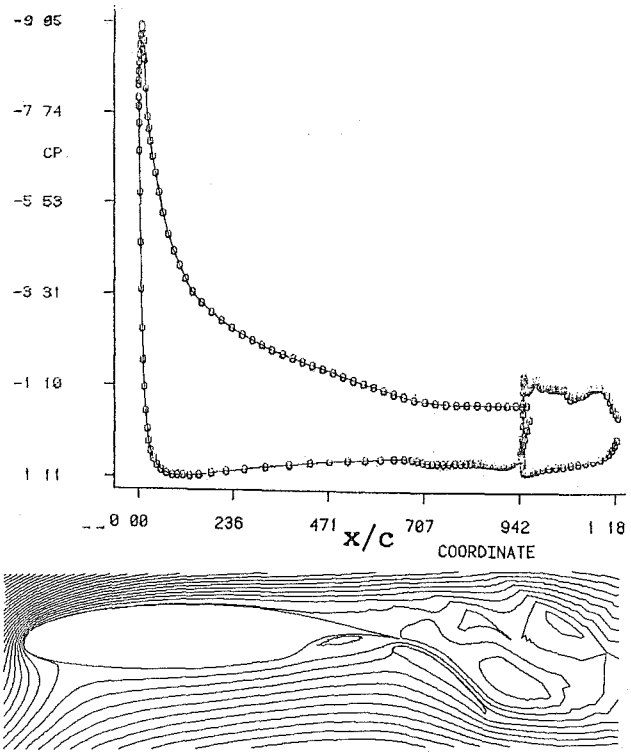

Fig.12 Streamlines and Cp, α = 15°, δ_f = 40°. GA(W)-1 multi-element.

At α of 10 degrees(the angle of maximum lift) the flow is attached on the flap and there is flow separation in the wake. As α is further increased the region of flow separation in the wake increases and approaches the wing. At α of 15 degrees there is separation from the wing trailing edge region with stall. The flow over the flap is attached even at stall conditions. This is seen also from flow visualization using tufts[7].The computations show that for high flap deflection the flow is separated over the flap and attached over the wing for small α, whereas at stall conditions the flow over the flap is attached and there is wake separation reaching the wing's trailing edge. This interesting flow behaviour was disscussed in an experimental investigation of flows over multi-elements[8].

For δ_f of 10 degrees the wing-flap gap is 2.3% and the overlap is 9.7% basic wing chord. We compute the flow for 0,10,12.5 angles of attack. The streamlines are shown in Fig.13,Fig.14 and Fig.15 respectively. It is seen that for zero α the flow is attached on the wing and flap surfaces. This is seen also from flow visualizations . As the angle of attack is increased the flow over the flap remains attached and flow separation begins in the wake and approaches the wing trailing edge region . Even at stall conditions the flow over the flap is attached (Fig.15) as also seen from flow visualization . At stall there is massive separated region in the wake reacing the wing's trailing edge region(Fig.15) as is also seen from flow visualization[7].

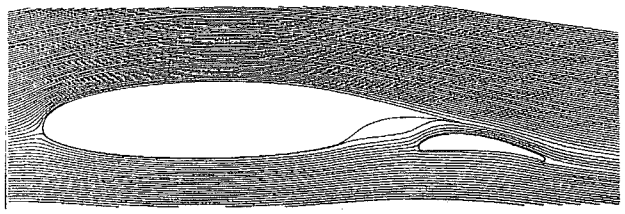

Fig.13 Streamlines and Cp, α = 0°, δ_f = 10°. GA(W)-1 multi-element.

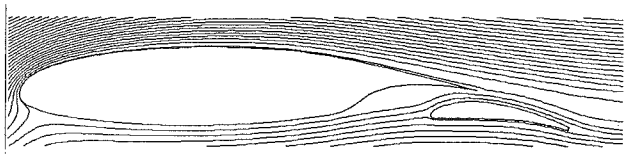

Fig.14 Streamlines and Cp, α = 10°, δ_f = 10°. GA(W)-1 multi-element.

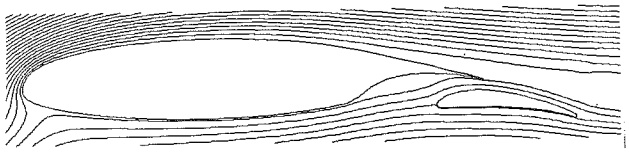

Fig.15 Streamlines and Cp, α = 12.5°, δ_f= 10°. GA(W)-1 multi-element.

NLR Multi-Element

The NLR wing-flap combination was investigated by Van den Berg[9]. It was composed of a supercritical main airfoil(NLR 7301) with flap having 32% basic wing chord length and a flap deflection of 20 degrees. The wing-flap was so designed that nowhere flow separations occurred, apart from an unavoidable small laminar separation bubble on the wing nose. A well streamlined shroud was designed to ensure attached flow along the shroud. The flap deflection of 20 degrees was close to the highest value that could be used without the onset of flow separation. The gap is 2.6% , the overlap is 5.3% basic wing chord and the test Re number is 2.5 millions. Boundary layer control by blowing was used to ensure two-dimensional flow conditions up to maximum lift. In the flow calculations we apply the slip condition on the wing and flap upper surfaces, where the flow is laminar and tune up the penalty and the upwinding parameters. Again, the tuning is simple : we take the smallest values for which we still have convergent solutions. Transition was fixed on all surfaces according to available experimental data.

Comparison of the computed C_L vs. α curve at Re number of 2.5 millions with the experimental curve is shown in Fig.16. It is seen that the agreement is good. The predicted C_{Lmax} is 3.02 and is 6% less than the experimental C_{Lmax} of 3.2 measured with blowing. As in Fosters's experiment ,when blowing is used to obtain two-dimensional flow conditions, the measured C_L is for all α greater by 5 to 8 percent than the predicted C_L using a Navier-Stokes code. It is interesting to compare the computed C_L vs. α curve with the curve computed by Cebeci[10] using an inviscid/viscid flow interaction analysis (Fig.17). Although there is no flow separation even close to C_{Lmax} on the configuration, the predicted C_L for α of 13 degrees is 7% higher than the experimental C_L measured with blowing. As will be shown, the separation leading to C_{Lmax} begins in the wake. Therefore, for the interaction analysis method it is very difficult to analyse strong interaction from wake separation and the computed C_L is almost linearly increasing with α for all α. A similar difficulty is seen also in the C_L vs. α prediction by B. Oskam using an interaction analysis method[11].

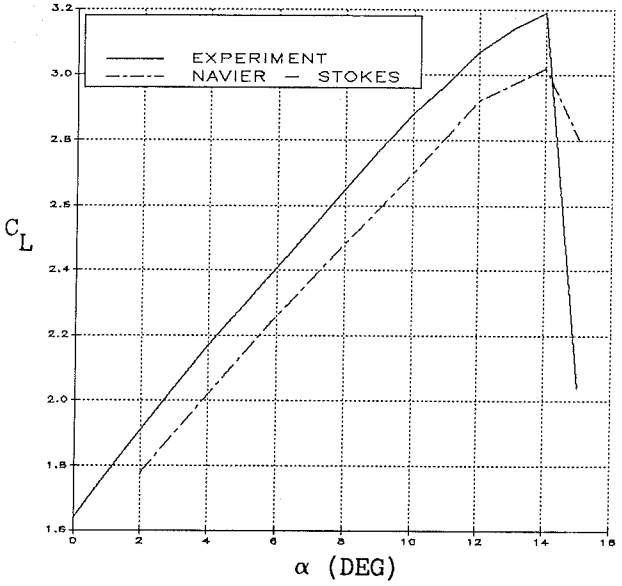

Fig.16 Comparison of computed C_L vs. α with experiment. NLR multi-element. Re = 2.5 million, δ_f = 20°.

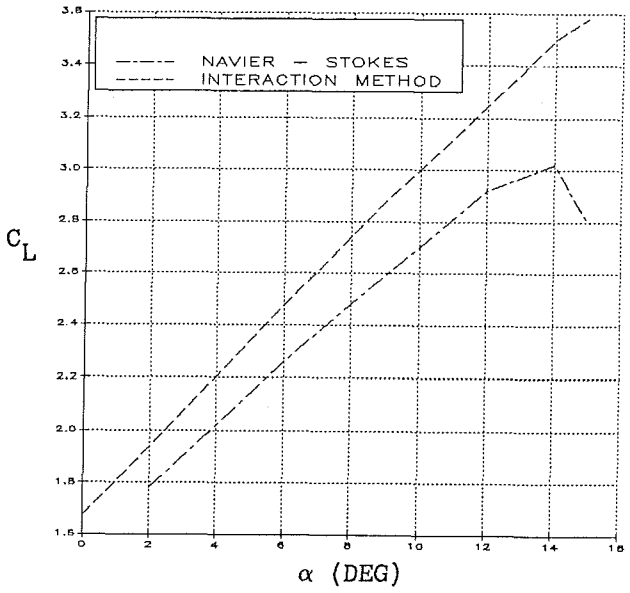

Fig.17 Comparison of computed C_L vs. α curves. Re = 2.5 million, δ_f = 20°. Cebeci's method vs. NAVIER-STOKES.

The streamlines of the flow for α of 13,14,15 degrees are shown in Fig.18. It is seen that the flow remains attached on the surfaces with flow separation developing in the wake of the main wing up to C_{Lmax}. The computed velocity field for α of 13 degrees is shown in Fig.19. It is seen that even close to C_{Lmax} the flow remains attached with a turbulent velocity profile still in the trailing edge regions on all surfaces.

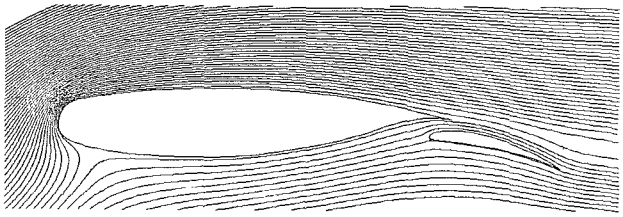

Fig.18 (a) Streamlines, α = 13°.

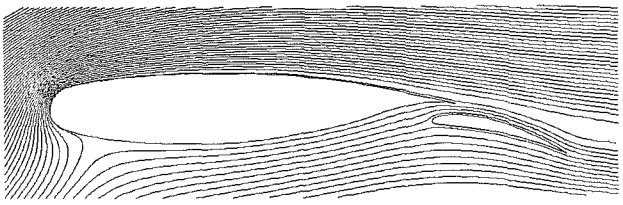

Fig.18 (b) Streamlines, α = 14°.

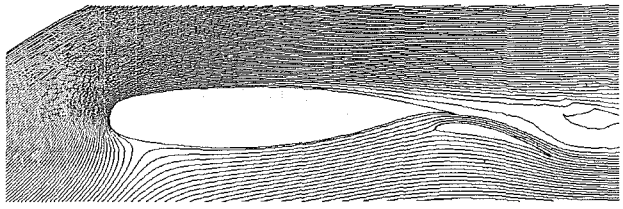

Fig.18 (c) Streamlines, α = 15°.

Fig.18 Streamlines for NLR multi-element. Re = 2.5 million, δ_f = 20°.

Comparison of computed Cp to experimental Cp at α of 6 and 13 degrees is shown in Fig.20. It is seen that the agreement is good everywhere with almost identical Cp on the lower surfaces. This is probably due to the fact that the effect of blowing on the lower surfaces flows is very small compared to the moderate effect on the upper surfaces' flows. The centre line of the wing's wake (defined as the line of minimum pitot profile issuing from the wing's trailing edge) as computed is compared to the experimental line for α of 6 degrees in Fig.21. Although no adaptive grid generation was used, it is seen that the wake is well captured.

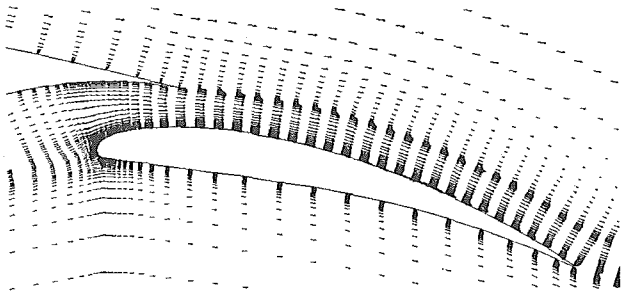

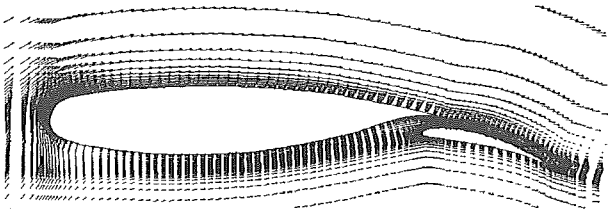

Fig.19 Computed velocity field, α = 13°. Re = 2.5 million, δ_f = 20°.

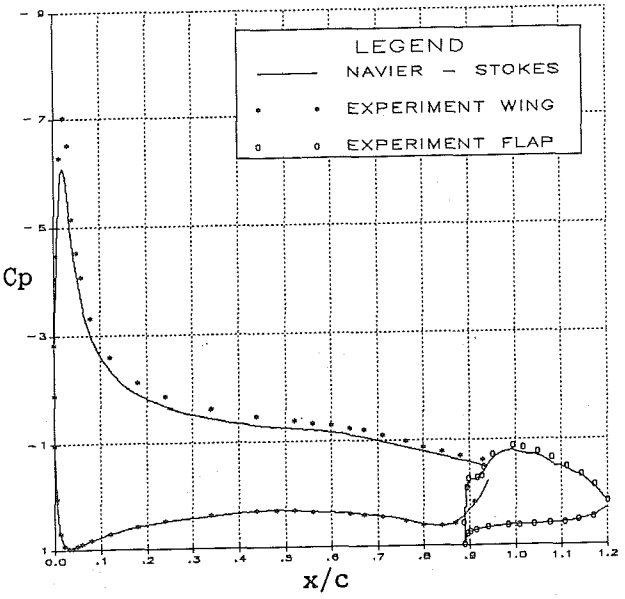

Fig.20 (a) NLR multi-element, Re=2.5 million, α = 6°

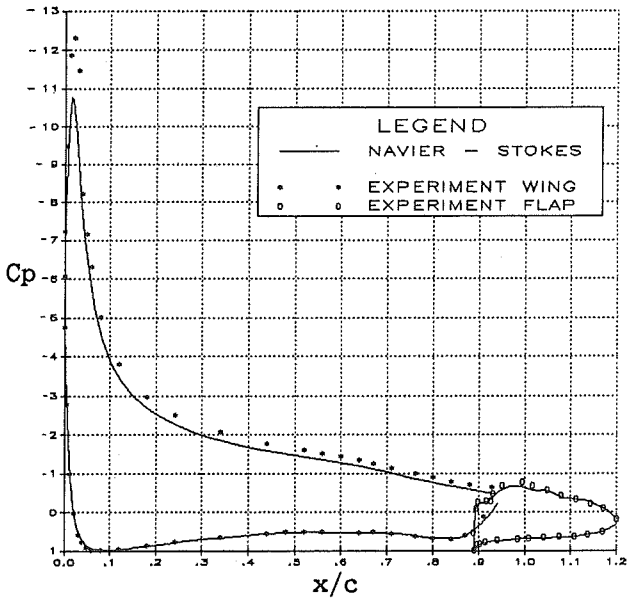

Fig.20 (b) NLR multi-element, Re=2.5 million, α = 13°

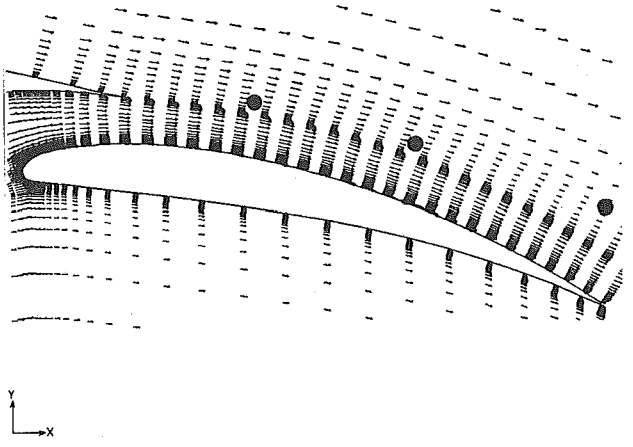

Fig.21 Wake center line from wing trailin edge.
● experiment.
NLR multi-element, α = 6°.

Comparison of computed boundary layer velocity profile with the experimental velocity profile for α of 6 degrees on the wing's upper surface at x/c=.6 and .94 (wing's trailing edge) is shown in Fig.22. The velocity Up is the potential velocity at the edge of the boundary layer. The measured values of Up are 1.5,1.25 at x/c=.6 and .94 respectively. The computed values are 1.42 and 1.2 at x/c=.6 and .94 respectively.

It is seen that in the inner layer the comparison is good and in the outer layer the measured velocity is higher than the computed velocity. This is partly due to lack of grid points as compared to measurements points in the outer layer and partly because of the blowing effect as disscussed above.

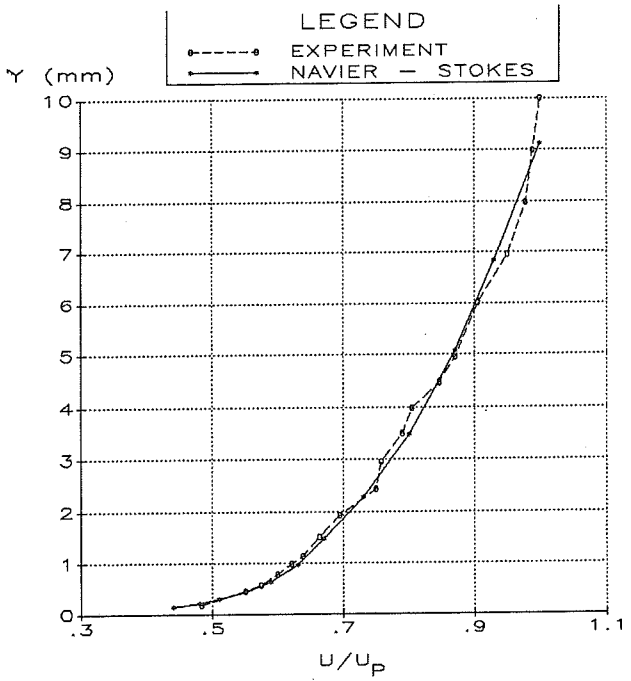

Fig.22 (a) Comparison of computed velocity to experiment.
Re =2.5 million, α=6°, x/c= .60.

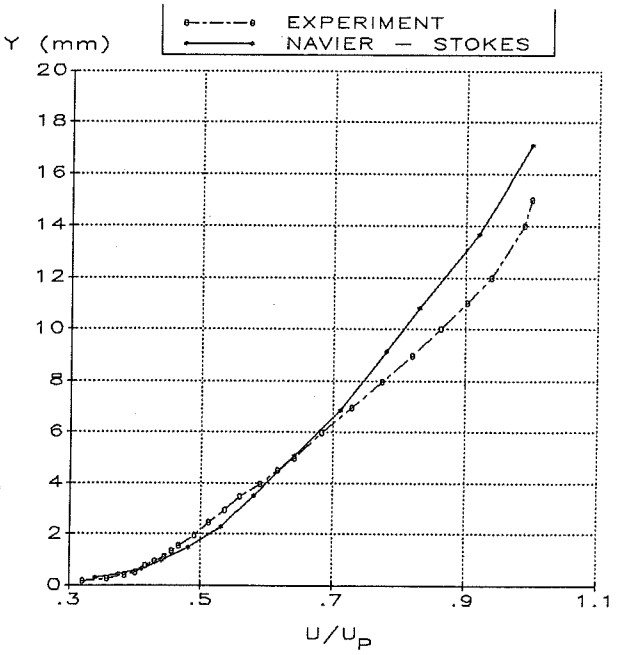

Fig.22 (b) Comparison of computed velocity to experiment.
Re =2.5 million, α=6°, x/c=.94.

PR8 Multi - Element

The PR8 multi - element was designed and tested in IAI. The flow was computed for Re of 1 and 1.5 millions about the wing-flap combination with zero flap deflection. In this flap position the wing-flap gap is about 1.2%. The computation of the flow in case of PR8 wing-flap is different from that about Foster or GA (W) multi-elements in two respects. First,since the basic airfoil is a laminar airfoil, the transition to turbulence follows the laminar separation bubble for all

angles of attack. Therefore, we must correctly predict bubble development throughout the laminar region. Secondly, the laminar boundary layer starting from the stagnation point at the leading edge of the main wing is resolved with sufficient accuracy on both wing surfaces by the same grid as used in case of GA(W)-1 multi-element(Fig.1). Therefore, there are no wiggles in the Cp calculations and we apply the no-slip condition on all solid surfaces including the laminar regions. In order to compute C_{Lmax} at Re number of 1.5 millions we must give transition location. For Re of 1.5 millions we take as the transition point the point of massive laminar separation that we get from a laminar flow calculation at the given Re and α. This resulted in transition locations for all α at Re of 1.5 millions between 18% and 23% basic wing chord.

The comparison of computed Cp to experimental Cp at C_L of 2.03 and al C_{Lmax} of 2.3 is shown in Fig.23 and Fig.24 respectively. It is seen that although the bubble is less pronounced than in the experiment, the agreement is reasonable and C_{Lmax} is predicted accurately as 2.3. However, the discrepancy between α used in the computation and the experimental α is 4 degrees. The streamlines of the flow at and beyond C_{Lmax} are shown in Fig.25. It is seen that the stall is due to flow separation from the trailing edge on the wing upper surface.

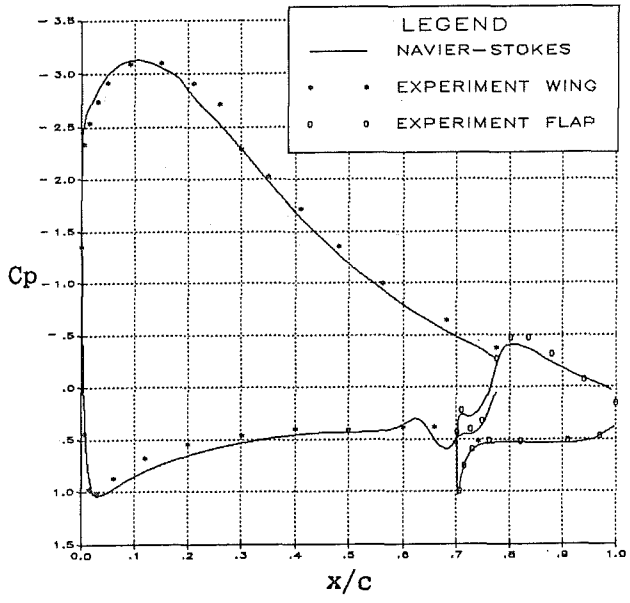

Fig.23 Comparison of computed Cp to experiment.

PR8 multi-element, C_L = 2.03, Re =1.5 million

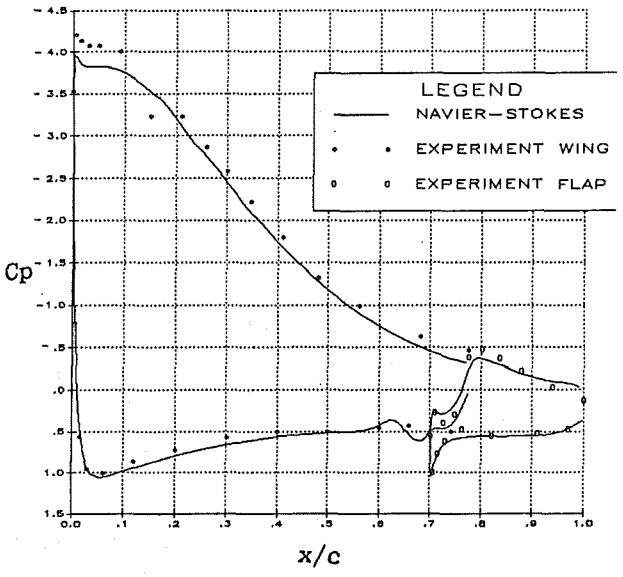

Fig.24 Comparison of computed Cp to experiment.

PR8 multi-element, C_{Lmax} = 2.3, Re=1.5 million

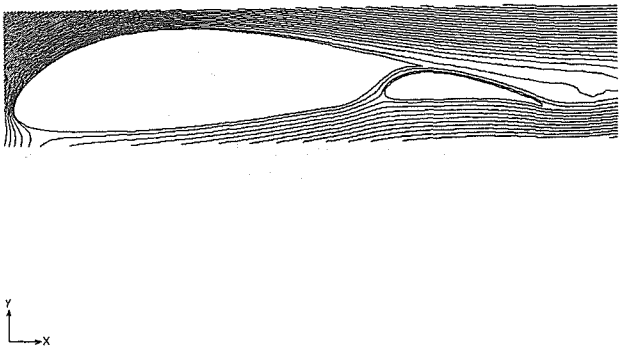

Fig.25 (a) Streamlines for flow at C_{Lmax}.
PR8 multi-element, Re=1.5 million, α = 18°

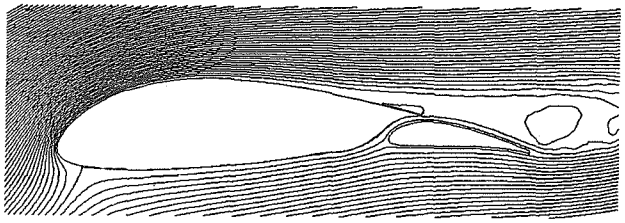

Fig.25 (b) Streamlines for flow at C_{Lmax}.
PR8 multi-element, Re=1.5million, α = 20°.

In case of Foster, GA (W) and NLR wing-flap combinations the comparison of computed Cp to experimental Cp at the same α gave reasonable results up to C_{Lmax} with differences of at most 8 percent. For these cases the wing-flap gap values were about 2.5% basic wing chord. In case of PR8, Cp comparison is for flap position with a relatively small gap of 1.2% which may contribute to the discrepancy.

In order to compute the flow about PR8 at Re of 1 million we apply the procedure for transition location[1] because the bubble is well pronounced. We assume a transition location at the point A on the wing upper surface of massive laminar separation that we get from the laminar flow simulation at the given Re and α. If after few iterations of turbulent flow simulation the flow is developing a laminar bubble with turbulent reattachment, we move transition point A towards the trailing edge and repeat the calculation with initial condition for the flow calculation the previous attached flow solution with transition point slightly upstream of A. This process is continued until the assumed transition location is such that there is a massive separation without reattachment. The point A in the process just preceding this point is taken as the point of transition to turbulence. This results in a convergent procedure both with regard to bubble location, bubble strength and Cp (Fig.26). The comparison of computed Cp to experimnent at C_L of 1.54 is shown in Fig.26. It is seen that Cp, bubble location and strength are well predicted. In this case the α used in the computation is 8 degrees, whereas the experimental α is 6 degrees giving 2 degrees discrepancy.

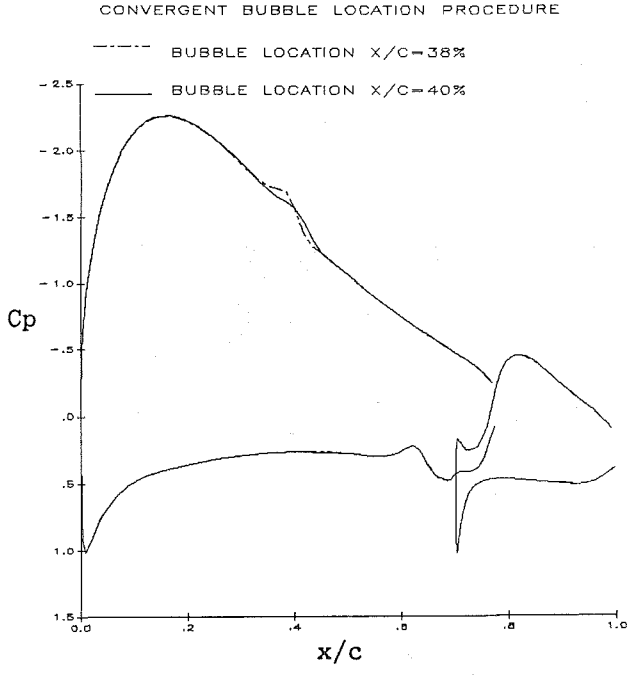

Fig.26 (a) Convergent bubble location procedure. Re = 1 million, C_L =1.54.

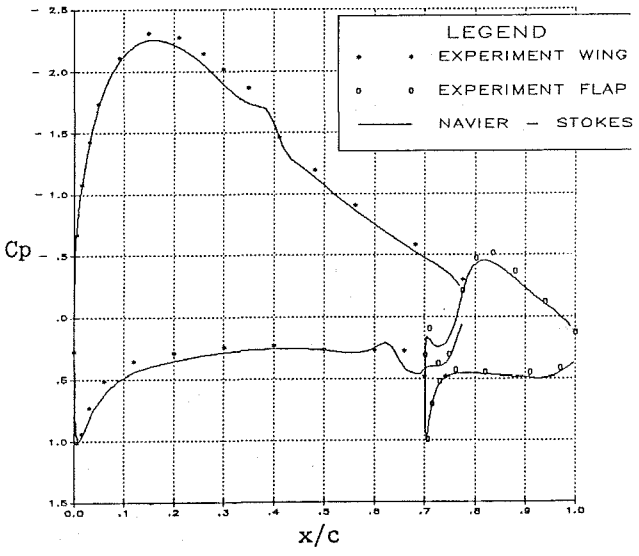

Fig.26 (b) Cp comparison, Re = 1 million C_L = 1.54.

We compare computed velocity profile in the boundary layer at the wing upper surface trailing edge with available experimental results at the Re number of 1 million and α of 2 degrees (Fig.27). It is seen that the agreement is good, indicating correct boundary layer prediction. To summarize the main points regarding the flow calculations for laminar PR8 wing-flap combination we have :

a) The α discrepancy increases with C_L.
b) For higher gap values (2.5% as opposed to 1.2%) such a discrepancy does not exist, computed Cp and experimental Cp agree reasonably at the same α.
c) Boundary layer prediction is reasonable.
d) At the same C_L, up to C_{Lmax}, Cp and bubble location comparisons are good.

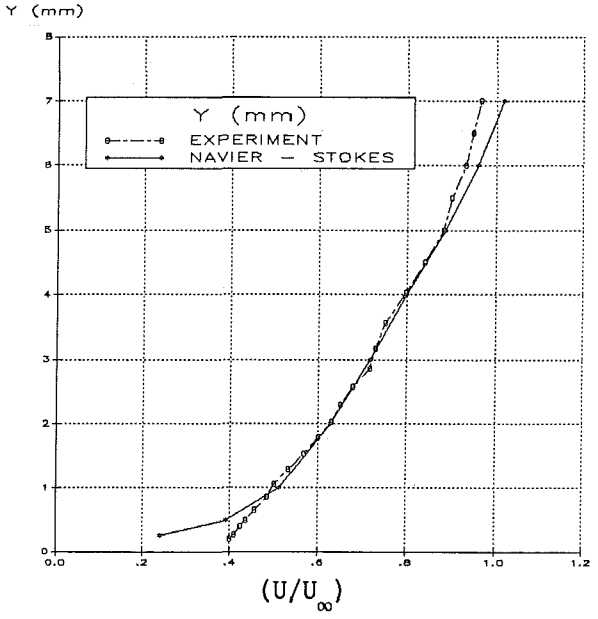

Fig.27 Comparison of computed velocity to experiment PR8 multi-element, Re=1 million, α = 2°. Wing's upper surface trailing edge.

Conclusions

The Baldwin-Lomax model was incorporated into the incompressible Navier-Stokes finite elements code FIDAP. The model was applied to compute turbulent flows over various wing-flap combinations for angles of attack up to maximum lift. The computed C_L vs. α curves and Cp are in reasonable agreement with experiments including C_{Lmax} predictions.

The Baldwin-Lomax model as applied is capable of treating turbulent flows with moderate separations.

An iterative convergent procedure was applied to compute the laminar bubble development over multi-element with laminar main wing.

An improved agreement with experimental results is obtained with tuning of the penalty and upwinding parameters.

For multi-elements which develop large pressure peaks at the leading edge of the main wing, it is necessary to suppress the wiggles in Cp by applying the slip condition in the laminar regions. This results in a much better agreement with experimental data.

References

1. A. Kogan and S. Migemi, 'The Calculation of Incompressible Separated Turbulent Boundary Layers', The Int. Journal for Numerical Methods in Fluids, VOL. 11, 39-56(1990).
2. B. S. Baldwin and H. Lomax, 'Thin Layer Approximation and Algebraic Model for Separated Flows', AIAA paper 78-257,1978.
3. FIDAP Users' Manual, Revision 4.0, Fluid Dynamics International, Inc. , September 1987.
4. D. N. Foster, H. P. A. H. Irwin and B. R. Williams, ' The Two-Dimensional Flow around a Slotted Flap', RAE Reports and Memoranda No. 3681, September 1970.
5. R. L. Sani, P. M. Gresho, R. L. Lee and D. F. Griffiths, 'The Cause and Cure of Spurious Pressures Generated by Certain FEM Solutions of the Incompresible Navier-Stokes Equations: Part 1 , The Int. Journal for Numerical Methods in Fluids, VOL. 1, 17-43(1981).
6. F. A. Dvorak and F. A. Woodward, 'A Viscous/Potential Flow Interaction Analysis Method for Multi-Element Infinite-Swept Wing', NASA CR-2476,November 1974.
7. W. H. Wentz, JR. and H. C. Seetharam, 'Development of a Fowler Flap System for a High Performance General Aviation Airfoil', NASA CR-2443,December 1974.
8. A. Nakayama, H.-P. Kreplin and H. L. Morgan, 'Experimental Investigation of Flowfield About a Multielement Airfoil', AIAA Journal, VOL. 28,No. 1, January 1990.
9. B. van den Berg, ' Boundary Layer Measurement on a Two-Dimensional Wing with Flap', NLR TR 79009 U, January 1979.
10. Tuncer Cebeci and K. C. Chang, R. W. Clark and N. D. Hasley, 'Calculation of Flow over Multielement Airfoils at High Lift', J. Aircraft, VOL. 24, No. 8,August 1987.
11. B. Oskam, ' A Calculation Method of the Viscous Flow around Multi-Component Airfoils', NLR TR 79097 U, September 1980.